Accretion disk dynamics, photoionized plasmas, and stellar opacities

R. C. Mancini,[1] J. E. Bailey,[2] J. F. Hawley,[3] T. Kallman,[4] M. Witthoeft,[4] S. J. Rose,[5] and H. Takabe[6]
[1]*Department of Physics, University of Nevada, Reno, Nevada 89557, USA*
[2]*Pulse Power Science Center, Sandia National Laboratories, Albuquerque, New Mexico 87545, USA*
[3]*Department of Astronomy, University of Virginia, Charlottesville, Virginia 22904, USA*
[4]*Goddard Space Flight Center, Code 662, National Aeronautics and Space Administration, Greenbelt, Maryland 20771, USA*
[5]*Department of Physics, Imperial College, London SW7 2BZ, United Kingdom*
[6]*Institute of Laser Engineering, University of Osaka, Osaka 565-0871, Japan*

(Received 22 September 2008; accepted 19 February 2009; published online 22 April 2009)

We present a brief review on the atomic kinetics, modeling and interpretation of astrophysical observations, and laboratory astrophysics experiments. The emphasis is on benchmarking of opacity calculations relevant for solar structure models, photoionized plasmas research, the magnetohydrodynamic numerical simulation of accretion disk dynamics, and a connection between radiation transport effects and plasma source geometry details. Specific cases of application are discussed with relevance to recent and proposed laboratory astrophysics experiments as well as Chandra and X-ray Multi-Mirror Mission Newton observations. © *2009 American Institute of Physics*. [DOI: 10.1063/1.3101819]

I. INTRODUCTION

Knowledge of astrophysical objects advances by observations, by constructing physical models to interpret observations, and by performing laboratory experiments that support the accuracy of both the models and the observation interpretation. This diverse approach to understanding is represented here by a brief review of recent laboratory opacity measurements aimed at reducing uncertainties in stellar interior models, photoionized plasma research, the accretion of powered objects that create photoionized plasmas, and an innovative approach to the link between radiation transport effects and plasma source geometry details. This work is based on a series of invited talks presented at the joint meeting held by the American Physical Society April Meeting and the High Energy Density Laboratory Astrophysics conference series that took place in St. Louis, Missouri in April 2008. Modern high-energy density (HED) laboratory facilities can now create photoionized plasmas and benchmark the spectral synthesis models used to interpret astrophysical photoionized plasma observations. They also can create and backlight plasmas hot enough so that their opacity becomes relevant for stellar modeling applications. Simultaneously, information of unprecedented detail is being provided by astrophysical observations and three-dimensional magnetohydrodynamic (MHD) numerical simulations. New opportunities to connect the models represented by the simulations and the observations are provided by increasingly comprehensive spectroscopic-quality atomic physics models that maximize the information that is extracted from the observations.

The interpretation of astrophysical observations often relies heavily on knowledge of the plasma properties. There are two complementary avenues that exploit this knowledge. First, plasma properties are used to build models for characteristics of the astrophysical object and those predicted characteristics are compared with observations. Second, interpretations of astrophysical objects can use spectral synthesis models that relate plasma properties to observed spectra. In the first case the plasma properties model is incorporated directly into the astrophysical object model and in the second case the plasma properties model enables data interpretation that then constrains the astrophysical object model. In both of these avenues, critical model tests and improvements can be provided by laboratory astrophysics. In this connection, we discuss experiments at Sandia National Laboratories pulsed-power Z facility, and at the GEKKO XII and Shenguang II high-power laser facilities that provide examples of these two different laboratory astrophysics approaches. The first avenue is exemplified in Sec. II by research investigating the spectrally resolved Fe *L*-shell opacity at temperatures above 100 eV; this measurement is important for testing and benchmarking theoretical opacities used in solar structure models. The second avenue is illustrated in Sec. III by experiments designed to test photoionized plasma kinetics and spectroscopy data analysis that are used to model and interpret line spectra from accretion powered objects. In order to wrap up the discussion on photoionized plasmas, Sec. IV overviews current challenges of astrophysical photoionized plasmas and, as an illustration, discusses the features observed in the absorption line spectrum of Active Galactic Nuclei (AGN) NGC3738 recorded by Chandra. Two methods for analysis of the observed line absorption spectrum and a critical discussion of the results are presented.

Recent advances in numerical algorithms have permitted more realistic and comprehensive models to simulate and study the dynamics of accretion powered disks. In this regard, we present in Sec. V the numerical simulation results from a state-of-the-art, three-dimensional code based on a relativistic, compressible MHD. Dynamical effects not explained by previous, steady-state analytical models are em-

phasized including the launching of plasma jets from accreting disks.

Finally, in Sec. VI, we look into yet another application of radiation transport to spectroscopic observations. In this case, the idea is to discriminate between different plasma source geometries by looking at the line ratio of optically thick and thin lines, i.e., line emission arising from atomic line transitions whose optical depth is larger or smaller than one, respectively. We show how this idea can be applied to observations from distant astrophysical plasma radiation sources where it is possible to perform spectrally resolved, spatially integrated emission measurements but it is not possible to record spatially resolved data.

II. LABORATORY ASTROPHYSICS AT Z: STELLAR INTERIOR OPACITIES

The breadth of the foundation provided by laboratory astrophysics is limited by the ability to recreate extreme HED environments on earth. Modern HED facilities are beginning to fulfill this need. The Z accelerator at Sandia National Laboratories[1] is one example. This device delivers more than 20 TW of electrical power to a few-centimeter-scale experiment, with a peak current above 20×10^6 A. This power can compress and heat plasmas that then generate intense x-ray bursts. The x rays are used to form a controlled HED plasma experiment.

A variety of configurations have been used for laboratory astrophysics experiments at Z (Ref. 2) (Fig. 1). The majority of these experiments have used ride alongs, in which the primary experiment goal was aimed at addressing some other topic such as Z-pinch physics or inertial confinement fusion. The available radiation and the geometrical configuration depend on the type of primary experiment. There are two main types of primary experiments that have been used for laboratory astrophysics: bare Z-pinch[3] and dynamic *Hohlraums*.[4] The bare pinch experiments typically use annular arrays of tungsten wires that implode onto the pinch axis and produce total x-ray peak power and energy up to roughly 200 TW and 1.5 MJ in a ~5 ns full width at half maximum (FWHM) pulse. In dynamic *Hohlraum* experiments the tungsten wire arrays implode onto a cylindrical 14 mg/cm^3 CH_2 foam placed on the pinch axis. This reduces the power emitted in the radial direction, but it forms a 12 mm tall 1–3 mm diameter cylindrical *Hohlraum* with radiation temperature that exceeds 200 eV.

The x-ray radiation incident on a laboratory astrophysics experiment depends on the total radiation generated and the geometrical configuration. Typically samples are placed to the side of bare pinch experiments at a radius 3–6 cm from the pinch axis. This provides an x-ray irradiance at the sample of approximately $0.3–5.0\times10^{12}$ W/cm^2; this is the case of the photoionized plasma experiment discussed in Sec. III. Samples placed to the side of dynamic *Hohlraum* experiments experience roughly half this irradiance. On the other hand, samples placed at the end of the dynamic *Hohlraum* are exposed to radiation brightness temperatures exceeding 200 eV, corresponding to irradiance values

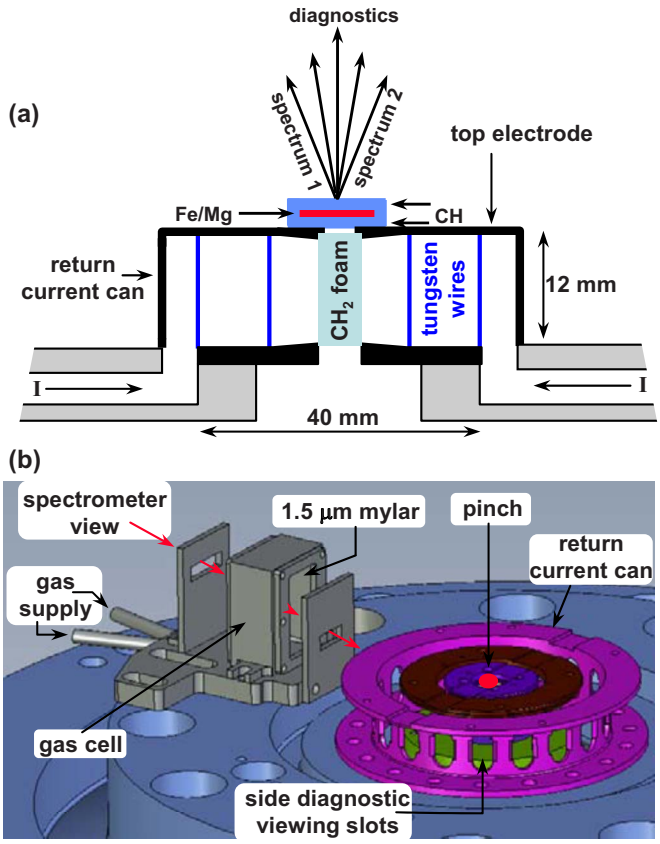

FIG. 1. (Color online) Schematics of experiment configurations used for laboratory astrophysics at the Z facility. The diagram in (a) shows the dynamic *Hohlraum* x-ray source used to investigate stellar interior opacities. The source is created when the annular tungsten wire arrays implode onto the CH_2 foam, generating and trapping radiation that heats the sample. The CH-tamped Fe/Mg sample located above the source is shown in an expanded scale for clarity. The diagram in (b) shows a bare Z-pinch configuration used to study photoionized plasma kinetics. The gas located ~5 cm from the pinch is photoionized by x rays that emerge from the diagnostic viewing slots when the pinch implodes on axis. The top pinch electrode structure is not shown.

exceeding 1.6×10^{14} W/cm^2. This is the configuration used in the opacity experiment discussed in this section.

In the sun, energy generated by nuclear reactions is transported outward by radiation over approximately 70% of the interior. The energy transport over the outer 30% is dominated by convection. The internal structure and the boundary location between the radiation and convection zones depend on the opacities. Presently, solar structure predictions do not agree with helioseismology observations.[5] Those predictions use opacities that have never been measured. The challenge is to create and diagnose solar interior conditions on earth, in order to evaluate whether this problem arises because of opacity model deficiencies or if it is due to some other aspect of the solar model such as the composition.

The solar region spanning radii $R\sim0.4–0.7R_0$ has been determined[6] to have the greatest influence on this discrepancy, where R_0 is defined as the exterior radius. In this region the temperature falls from 293 to 182 eV and the electron density falls from 4×10^{23} to 9×10^{22} cm^{-3}.[5,6] The elements expected to influence the opacity the most in this region are oxygen, neon, and iron.[5] In our work we have focused on

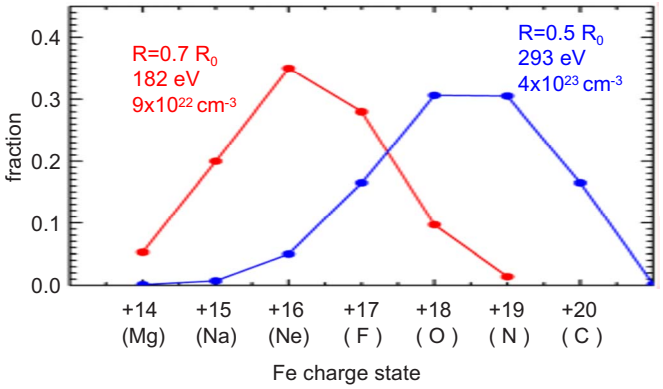

FIG. 2. (Color online) Charge state distribution calculated for iron in the solar interior. The indicated radii, electron temperature, and electron density are from Ref. 6 and the calculations were performed with PRISMSPECT (Ref. 7).

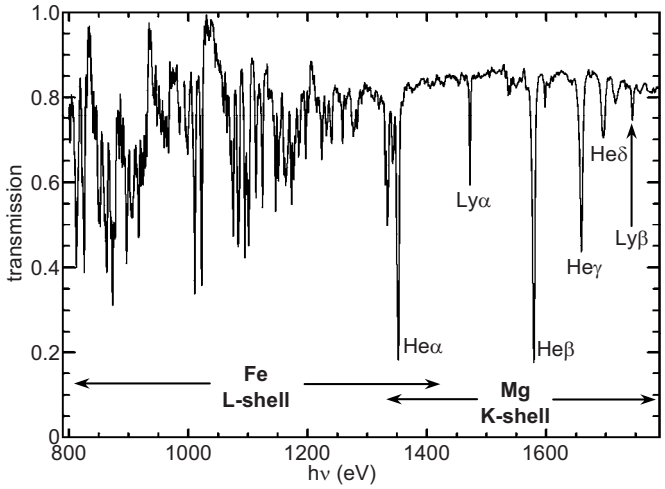

FIG. 3. Transmission measured for a mixed Fe/Mg plasma at electron temperature $T_e = 156 \pm 6$ eV and density $N = 6.9 \pm 1.7 \times 10^{21}$ cm^{-3}. The transmission in the 800–987 eV range corresponds to a thin Fe sample and the transmission in the 992–1790 eV range corresponds to a thicker Fe sample (see Ref. 10). The Mg K-shell transitions are used to diagnose the plasma, enabling tests of opacity model calculations for the Fe *L*-shell transitions.

iron because it has a higher atomic number, correspondingly higher atomic complexity, and therefore is more challenging to model accurately. A prerequisite to test opacity models is the ability to produce the relevant charge states. The iron charge state distribution for solar interior conditions was calculated using the PRISMSPECT (Ref. 7) spectral analysis code (Fig. 2). The Ne-like, F-like, and O-like ionization stages are abundant over a broad range of solar interior conditions. Therefore, laboratory experiments must aim to produce these charge states and then to measure plasma transmission. An evaluation of the contributions from the different elements indicates that the most important photon energy range for iron is the 700–1800 eV range that encompasses the *L*-shell bound-bound and bound-free transitions.

Opacity experiments typically use x rays to heat a sample and measure the sample transmission by viewing a backlighter through the sample with a spectrometer.[8] The requirements for such experiments are well established.[9] However, meeting the requirements becomes more demanding as the temperature increases because the energy density needed to heat the sample goes up and the backlighter brightness needed to overwhelm the sample self emission also goes up. The first opacity experiments hot enough to measure transitions in the iron charge states that occur in the solar interior were reported in Ref. 10.

The Ref. 10 experiments used a CH tamped Fe/Mg sample, i.e., a Fe/Mg mixture placed in between two plastic slabs 10 μm thick each, that was both heated and backlit by the Z dynamic *Hohlraum* x-ray source [Fig. 1(a)]. The transmission was obtained by comparing experiments with and without the Fe/Mg portion of the sample and exploiting the reproducibility of the experiments (Fig. 3). The $\pm 2\%$–5% relative transmission accuracy was achieved by averaging multiple reproducible experiments. Self-emission was rendered unimportant by the high spectral radiance of the dynamic *Hohlraum* backlighter, roughly equivalent to a ~ 314 eV brightness temperature.[11] The backlighter provides a broad spectral range absorption spectrum, suitable for simultaneous measurements of the Mg *K*-shell and the Fe *L*-shell transitions. The Mg *K*-shell transitions are relatively well understood and provide diagnostics for the plasma conditions. The electron temperature is inferred from the relative absorption strength of transitions in He-like and H-like Mg and the electron density is inferred from the Stark broadened He-like Mg $1s^2-1s3p$, $1s^2-1s4p$, and $1s^2-1s5p$ profiles. The ability to reproduce the experimental transmission at a single temperature and density is consistent with uniform plasma. Comparisons of the Fe *L*-shell transmission with the PRSIMSPECT,[7] OPAL,[12] MUTA,[13] and OPAS (Ref. 14) detailed opacity models exhibits an impressive level of agreement. The average difference between the models and the data was approximately 8% in the 1005–1320 eV photon energy range and 10%–16% in the 800–1005 eV range. Statistically significant differences do exist for specific spectral features and the possibility of residual systematic experiment errors or model deficiencies remains under investigation. Furthermore, the good agreement obtained with the four detailed models does not necessarily imply that models used for applications such as the solar interior also possess high accuracy. The comparison in Ref. 10 used model calculations that could afford to devote attention to calculating single element opacity at a single value of temperature and density. Applications require multiple element opacities computed at a broad temperature and density range. For example, a 20 element mixture is typically used in solar models. Work is ongoing to exploit the measurements and modeling results obtained in this research to help evaluate the accuracy of stellar interior opacity models. This work will be published elsewhere. These initial laboratory experiments provide the ability to examine many important aspects of the opacity models, including charge state distribution, bound-bound transition bundling into unresolved arrays, inclusion of multiply excited states, and inclusion of low probability transitions. Tests of some issues such as line broadening will require further experimental advances.

III. PULSED POWER AND LASER-DRIVEN PHOTOIONIZED PLASMAS

Quantitative astrophysical model tests rely on comparisons with images and emission or absorption spectra. The spectrum emitted or absorbed by any plasma is extremely sensitive to the charge state distribution, which is dominated in many astrophysical plasmas by photoionization.[15] Examples include active galactic nuclei, x-ray binaries, and black hole accretion disks. These plasmas are typically subjected to a powerful external radiation source and the density is low enough that radiation driven processes cause ionization at a rate much faster than electron collisional ionization. This implies that accurate model constraints depend on accurate models for interpreting photoionized plasma spectra. Unfortunately, to date almost all laboratory experiments have collision dominated ionization and very few tests of photoionized plasma spectral synthesis models exist.

Insufficient x-ray source brightness is the main reason for the dearth of laboratory photoionization studies. Photoionized plasmas are characterized by the ionization parameter[15,16] $\xi=4\pi I/N$, where I is the irradiance (erg/cm^2 s) at the plasma and N is the electron density in cm^{-3}. The photoionization parameter represents the degree of overionization caused by the radiation, relative to the ionization characteristic of a collision-dominated plasma. In astrophysical photoionized plasmas, $\xi\sim 1-1000$ ergs cm/s. Testing photoionization models in the laboratory requires high irradiance and low density. However, the ability to diagnose the plasma requires a sufficient number of emitting or absorbing atoms and the density can therefore not be arbitrarily low. Thus, effective laboratory experiments require the highest possible irradiance and the largest possible plasma size.

The new generation of HED facilities such as Z can help to fill this need as they are able to generate higher x-ray fluence over larger spatial scales. The first photoionization kinetics experiments at Z (Ref. 17) used 500–750 Å thick Fe/NaF foils that were located 1.5 cm to the side of bare tungsten Z-pinch plasmas. The Z-pinch run-in radiation vaporized the foils, causing them to expand to a $\sim 2\times 10^{19}$ cm^{-3} electron density. The main Z-pinch radiation pulse exposed the low density plasma to $\xi\sim 25$ ergs cm/s and the foil characteristics were measured with absorption spectroscopy. The charge state distribution inferred from the absorption spectra enabled tests of the CLOUDY,[18] NIMP,[19] and GALAXY (Ref. 19) photoionization codes.

Subsequent photoionization experiments[20,21] at Z used prefilled gas cells to expose neon gas to x rays with a peak photoionization parameter $\xi\sim 5-7$ ergs cm/s. These gas cell experiments [Fig. 1(b)] offer several advantages: O, Ne, and Ar appear in astrophysical spectra and are most conveniently tested in gaseous form, a desired low density can be preselected, the relatively large 1–2 cm scale plasma promotes high quality signals, and there are no Doppler effect complications that influence the interpretation. The main challenge to be overcome is the need to avoid collecting diagnostic signals from the shocks launched when the Mylar windows absorb incident radiation. In addition, the uniformity of larger plasmas must be carefully evaluated since geometrical dilution of the radiation may become more serious as the sample size increases.

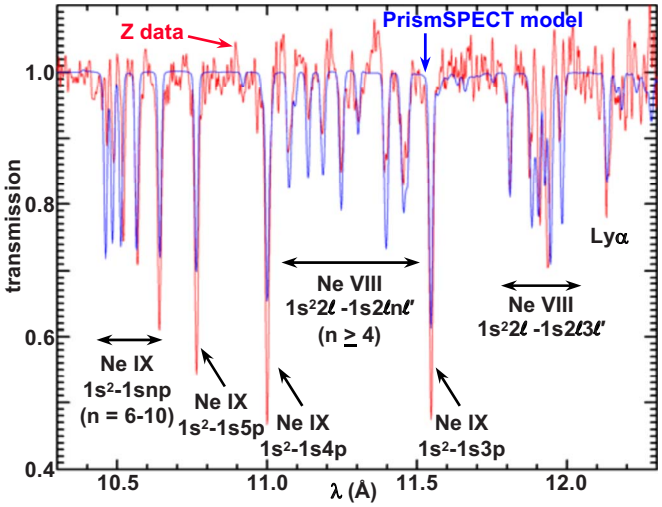

FIG. 4. (Color online) Transmission measured for a photoionized neon plasma. PRISMSPECT model calculations are superimposed on the data.

The Z photoionized neon plasma transmission T exhibits absorption features from H-like, He-like, and Li-like neon (Fig. 4). A noteworthy aspect of these experiments is that the 10^{18} ions/cm^2 areal density is similar to astrophysical plasmas. Line identification in astrophysical plasmas is complicated by the presence of multiple elements that contribute spectral features that may overlap. Thus, laboratory measurements with a known single constituent may provide valuable information concerning the absorption line wavelengths and relative intensities. Initial comparisons of the data with nonlocal thermodynamic equilibrium PRISMSPECT calculations possess a promising level of agreement. The Li-like $1s^22l-1s2l3l'$ and $1s^22l-1s2l4l'$ complexes are reasonably well reproduced, as are the Lyα and some of the He-like transitions. The calculated transmission T of the He-like $1s^2-1snp$ lines with $n=3-6$ is too large by $\Delta T\sim 0.1-0.15$ and the calculated transmission T of the He-like $1s^2-1s9p$ and $1s^2-1s10p$ lines is too low by $\Delta T\sim 0.1-0.15$. Investigations of these issues and comparisons with models used for astrophysical analysis (such as CLOUDY) are ongoing work. Future experiments will include the possibility of time-resolved determination of the charge state distribution evolution, evaluation of spectral signatures present in emission spectra, the variation in charge state distribution as the density is further reduced, and configurations that provide higher irradiance values. The addition of Thomson scattering to provide an independent electron temperature diagnostic is also under consideration.

Next, we turn our attention to laser-driven photoionized plasma experiments. First, we consider an experiment performed in the Shenguang II laser facility in Shanghai, China where a silicon gel sample placed in a "dog-bone" shaped *Hohlraum* cavity was driven by eight laser beams entering the *Hohlraum* in two groups of four beams each through both ends of the cavity, as displayed in Fig. 5.[22] The dog-bone shaped *Hohlraum*, which has cylindrical symmetry and

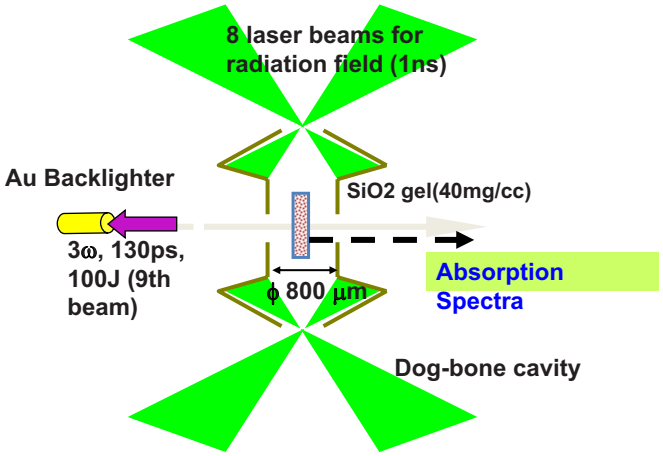

FIG. 5. (Color online) Schematic of the dog-bone shaped *Hohlraum* cavity and backlighter source for laser-driven photoionized plasma experiments.

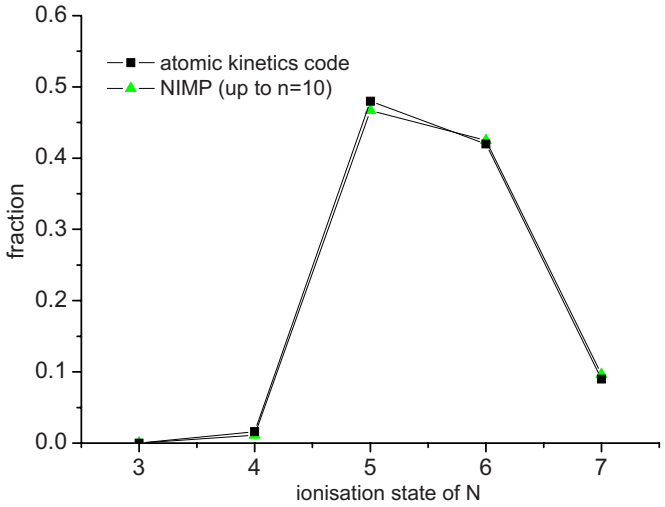

FIG. 6. (Color online) Comparison of fractional populations for a nitrogen photoionized plasma with results computed with the NIMP code (Ref. 19).

it is approximately 2.5 mm long by 0.8 mm in diameter, prevents the laser beams from directly interacting with the silicon gel inside the main body of the *Hohlraum*. It is the *Hohlraum* radiation field that actually heats and ionizes the silicon gel thus turning it into a photoionized silicon plasma. The plasma was backlit with the x-ray flux from a gold laser-produced plasma, and the transmission spectrum through the silicon plasma recorded for detailed spectroscopic analysis. In a first approximation, the interpretation and modeling of the data assumed Saha equilibrium ionization and level population distribution with detail term accounting description of the energy level structure.[23] Energy level and ionization potential values were computed with the flexible atomic code atomic structure code.[24] The transmission spectrum included absorption arising from $1s^2 2l^m n'l'$ to $1s^2 2l^{m+1}$ line transitions, where m is in the range from 1 to 8 in Be-through Na-like Si ions, and the spectral line shapes were Voigt profiles with a width dominated by instrumental broadening effects (FWHM ~0.89 eV). From the spectroscopic analysis of the transmission spectrum we extracted a density of 10 mg/cm^3 and temperature equal to 56 eV, which is less than the radiation temperature (i.e., 80–100 eV) in the cavity. Also, it was possible to determine that 70% of absorption was due to ions in the ground state configuration (i.e., $n'=2$), 20% was due to excited ions with $n'=3-6$, and less than 5% from excited ions with $n'>6$.

Another important aspect of photoionized plasma research is the observation and spectroscopic analysis of the radiation emitted by the plasma, i.e., the self-emission of the plasma.[25,26] In this connection, we discuss an experiment fielded at the GEKKO XII laser facility of the Institute of Laser Engineering at Osaka University, Japan.[27] In this experiment, the target was a gas-bag filled with nitrogen and placed inside a gold-coated dog-bone shape *Hohlraum* cavity, similar to the one used at the Shenguang II laser facility. The filling pressure of the gas bag is such that the nitrogen number density is 1.4×10^{19} cm^{-3}. The almost Planckian radiation flux inside the cavity (radiation temperature of about 80 eV) drives the nitrogen gas turning it into a photoionized plasma. The time evolution of the He- and H-like emission line spectra was recorded with a time-resolved spectrometer, and He- to H-like N ion line ratios were used to extract the plasma temperature. To this end, we have developed an atomic kinetics rate equation solver with detailed configuration accounting based on the screened hydrogenic atom approximation. The line transition energies and oscillator strengths were calculated with the HULLAC suite of atomic codes.[28,29] From the analysis of the line ratio data we were able to determine and electron and ion temperature of approximately 20 eV. The fractional populations of the plasma are displayed in Fig. 6, which also includes a comparison with results from the NIMP code.[19] The calculations were done for a density of 0.325 mg cm^{-3}, electron and ion temperatures of 20 eV, and radiation temperature of 80 eV. The next step in the development of this code will be to include inner-shell direct photoionization for treating plasmas made out of higher atomic number elements and relatively high radiation temperatures (~1 keV), as in the case of compact stars.[25,26] Also, we are currently assuming that the bound electrons are in the ground state with only one electron in an excited state. In cases of high radiation temperature, *K*-shell electrons can also be ionized with x rays of energies higher than the ionization threshold. Work is currently in progress to extend the atomic kinetics model to include this effect.

IV. CURRENT CHALLENGES OF ASTROPHYSICAL PHOTOIONIZED PLASMAS

Photoionized plasmas exist in the vicinity of very exotic and interesting astrophysical objects, such as black holes and neutron stars which are fueled by accretion. While these objects are too distant to be imaged, spectra from these sources are rich in absorption features. The spectra can give us information about elemental abundances, temperatures, and general kinematics of the accreting gas. From this information we hope to gain insight on object at the center of the plasma, e.g., relativistic effects, magnetic processes (Blandford-Znajek, Poynting flux), and the physics near the surface of the compact object. In order to accomplish these goals, a

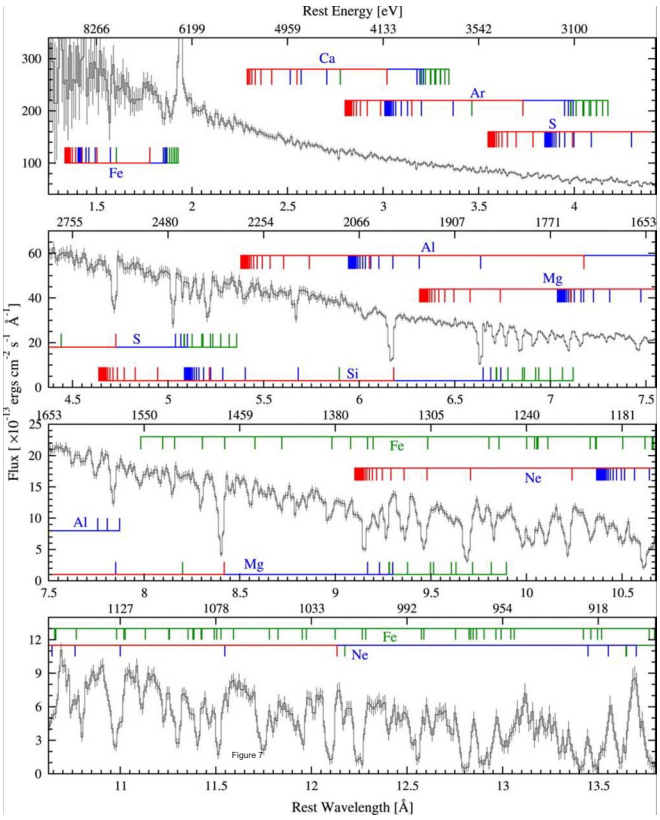

FIG. 7. (Color online) Absorption line spectrum recorded by Chandra from AGN NGC3738 in the wavelength range from 1.25 to 13.8 A.

solid understanding of photoionized plasma spectra must first be established which requires good atomic data and accurate models.

The first x-ray spectra of active galaxies from HEAO-1 (1978) revealed simple power law spectra at high energies. Successive satellites found, however, that the x-ray spectra from these sources started to deviate from neutral absorption at low energies suggesting that there was at least some partially ionized species in the gas. This was confirmed by the Japanese ASCA satellite (1993) which discovered absorption edges of partially ionized oxygen in the low energy spectra. Now with the Chandra and X-ray Multi-Mission (XMM) satellites (1999) we have detailed spectra that can be thoroughly compared to plasma models. For example, a 900 ks observation of AGN NGC3738 with Chandra (see Fig. 7) revealed over 100 line absorption features.[30] These features are found to be blueshifted with a Doppler velocity of 800 km/s, and also broadened. It is customary to model this broadening as turbulence, with a Maxwellian distribution and a characteristic velocity (sigma) of 300 km/s. This suggests an outflow of the ionized gas and some large scale dynamics leading to the broadening. Such spectra have been obtained from several AGNs.

From a theoretical perspective, the population of the various ionized species in the plasma is determined by balancing the rates of ionization with recombination. We are assuming that the gas is in equilibrium, so any time dependence of the populations is neglected. In contrast to high-density coronal plasmas which are dominated by electron collisions, it is photoionization and a combination of dielectronic and radiative recombination which govern the populations for photoionized plasmas. The system must also satisfy radiative equilibrium that is the heating rate of the plasma due to the slowing down of photoelectrons must be balanced by the cooling rate from excitation, recombination, etc. This additional constraint means that the temperature is no longer a free parameter, instead it is a function of the density of the plasma and incoming radiation flux. Therefore, when modeling a photoionized plasma, the important physical parameter is the ionization parameter ξ, as defined in Sec. II.

In Fig. 8, we show typical ionization balance plots for several species. From these kind of plots, we can determine the relative abundances of the ions for a given ionization parameter ξ. In practice, however, we first determine the abundances from the observed lines in the spectra and use these figures to infer the ionization parameter. By repeating this procedure with several lines, we can gain confidence in our value for the ionization parameter and determine whether the plasma is better described by a distribution of ionization parameters rather than just a single component.

One straightforward way to fit a spectrum for an AGN without assuming any knowledge of the underlying physical processes, is to fit each absorption feature with a simple Gaussian. For the spectrum of NGC3738 (see Fig. 7), this procedure requires about 950 lines of which 100 are currently identified and can be used to obtain abundances. Using the ionization balance curves from Fig. 8, we find that the ionization parameter for this system lies between $10^{1.5}$ and $10^{2.5}$ ergs cm/s.

A more satisfying way to fit this spectrum is to apply the photoionization model discussed above to generate a synthetic spectrum. This synthetic spectrum is calculated iteratively until the best fit with observation is obtained by adjusting the ionization parameter, outflow velocity, and turbulent velocity. This approach can fit features not observable as individual lines as well as absorption edges. The result of this procedure with NGC3738 yields an ionization parameter of 10^2 ergs cm/s, which is in good agreement with the result obtained using the Gaussian fits.

Despite the overall good agreement between the synthetic and observed spectra for NGC3738, there are some areas of disagreement. Two of these areas are highlighted here. Between 16A and 17A, there are several observed absorption features which are not predicted by the model. These features were found to be from $n=2-3$ transitions of Fe I to Fe XV. These M-shell unresolved transition array lines are sensitive to the ionization parameter and it is found that an ionization parameter ξ of 1 erg cm/s provides the best fit with the observed spectrum. This result implies that the photoionized gas has either two components in terms of the ionization parameter or that it has a broad continuous distribution of ionization parameter covering at least two orders of magnitude. Both of these scenarios were tested and the two-component fit resulted in good agreement with the observation while the continuous distribution of ionization parameter showed severe overabsorption.

Another region of disagreement is between 6.5 and 7 A, where again absorption features seen in the observed spec-

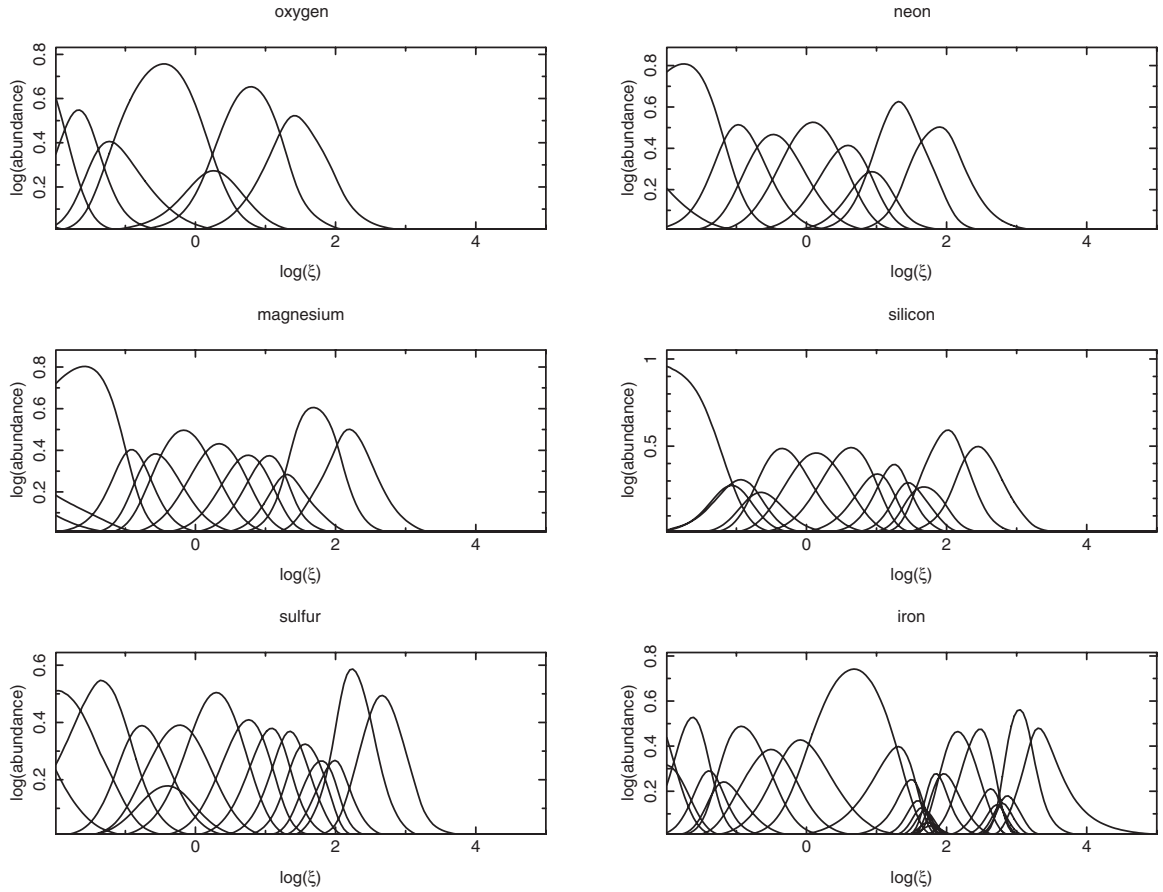

FIG. 8. Ionization balance distributions for oxygen, neon, magnesium, silicon, sulfur, and iron. Each plot displays the total fractional population per ionization stage as a function of the ionization parameter ξ in erg cm/s.

trum were not reproduced by the model. In this case, it was the atomic data in the model at fault. Specifically, the low temperature dielectronic rates for Fe were found to be too low by a factor of 2–5. Using new dielectronic rates, we find much better agreement between the synthetic and observed spectra in the 6.5–7A range.

While good agreement is found between the photoionized model and observations, it is not yet good enough to fathom the dynamics of the plasma. Most models to date fit these spectra by assuming a simplistic two or three component model approximation. In some objects, however, there appears to be a gap in the ionization distribution while others seem to have gas over a wide range of ionization parameter. Better atomic data are needed to fit more features of the spectra and pin down the physical parameters of these systems.

V. ASTROPHYSICS OF ACCRETION ONTO COMPACT OBJECTS

The most energetic phenomena in the universe are systems powered by gravity through accretion. When matter of mass m falls down onto the surface of an object of mass M and radius R it can release $\sim GMm/R$ of gravitational potential energy. For compact stars such as white dwarfs, neutron stars, and especially black holes, the mass M is large and the radius R is small and the energy released per unit mass accreted can be comparable to or greater than that released by nuclear reactions.

Accretion plays a significant or even dominant role in many high energy astrophysical systems, from stellar-massed compact binary systems up to the supermassive black holes that power quasars, AGN and radio jets. Space- and ground-based observations are providing increasingly detailed information about accreting systems. For example, the spectral energy distribution and luminosities seen in x-ray binaries and AGN are strongly variable, often with substantial amplitudes on short timescales comparable to the orbital time near the central black hole. Many x-ray binaries show dramatic spectral variability, from thermal emission dominated by soft x rays to states characterized by nonthermal emission in hard x rays.[31] Jets are seen in many systems; their ubiquity suggests that they can be produced under quite general conditions.

It is clear that accretion systems are highly dynamic. But until recently the theory of black hole accretion has been based primarily on a one-dimensional time-steady model consisting of an optically thick, vertically thin, Keplerian disk with an unknown, parametrized internal stress.[32,33] While this analytic model successfully accounts for some properties of accretion systems, particularly the thermal continuum emission, its limitations are well known. Numerical

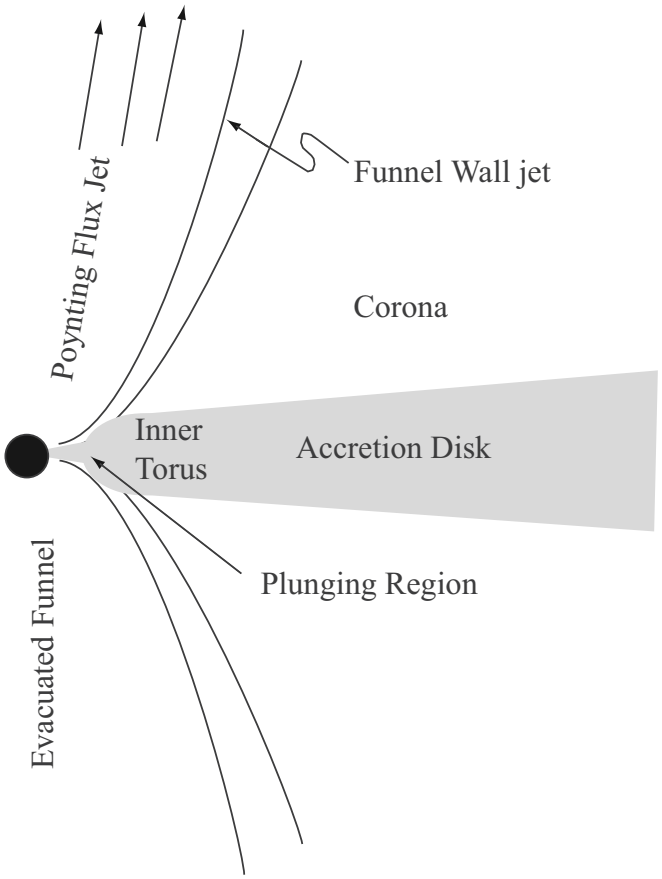

FIG. 9. Schematic illustration of the main dynamical features seen in accretion disk simulations. From Ref. 41 [J. F. Hawley and J. H. Krolik, Astrophys. J. **641**, 103 (2005)], copyright © The American Astronomical Society. Reprinted by permission of The American Astronomical Society.

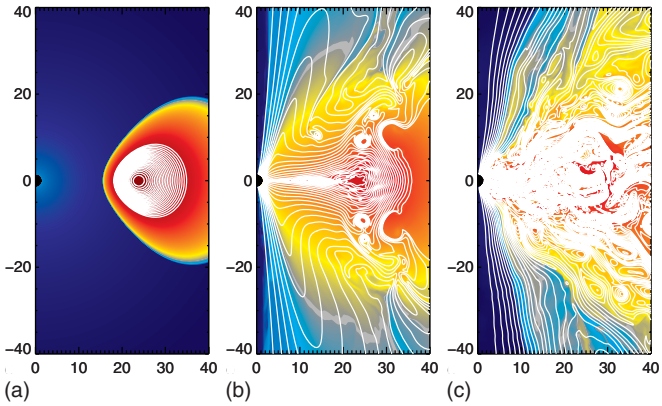

FIG. 10. (Color online) Evolution of magnetic field (white contours) and gas density (color contours) in a three-dimensional simulation beginning with an orbiting gas torus containing dipole magnetic field loops. (a) The initial condition. (b) At time $500M$ the field has been brought down to the black hole and has begun to fill the axial region. (c) By time $3000M$ the field has become highly tangled within the accretion disk and coronal region, but along the axis the field is regular and mostly radial with a toroidal component due to the rotation of the black hole.

simulations provide a way to go beyond the standard model and investigate the detailed dynamics of accretion flows. This is possible in part because the nature of the internal stress is no longer unknown. Angular momentum transport within accretion disks is accomplished by the magnetorotational instability,[34] a local, linear, and rapidly growing instability. Because of this the governing equations are those of compressible MHD, and those equations are the starting point for developing detailed models of accretion dynamics. For the past several years we have been developing and applying a three-dimensional general relativistic MHD code to the problem of accretion into spinning black holes. The code[35] has produced a significant number of accretion simulations run for extensive periods of evolution time. The time and length scales involved in accretion simulations make such simulations challenging, but even with current limitations, the first results have revealed details about time-dependent properties of disks, magnetic disk dynamos, jet launching mechanisms, and the dynamical properties of systems other than the standard thin disk.

We have found that certain dynamical components tend to arise naturally in MHD turbulent black hole accretion systems.[36] Figure 9 presents a schematic of these features which include the accretion disk itself, a surrounding magnetized corona, and an unbound jet along the black hole axis. There are also significant dynamical effects near the black hole that are not present in simple analytic models. In particular, and contrary to the expectations of traditional accretion disk theory, there is no general surface within which the stress in the inflow vanishes.[37,38] This can result in significant increases in accretion efficiency for holes with low spin values.[39] Further, a strongly spin-dependent outward flux of angular momentum conveyed electromagnetically from the hole to the accretion disk can retard the effective accretion rate for Kerr holes.[37]

The axial jet seen in many of the simulations is of particular interest. While it is widely accepted that large-scale magnetic fields, if present, can launch jets from an accretion disk, our simulations[35–40] have demonstrated jet creation from a disk without a pre-existing large scale field. This is illustrated in Fig. 10 which shows the evolution of an initial gas torus containing dipole loops of weak field (plasma β value of 100). The field is carried in by the accretion process and then ejected into the empty axial funnel. At late times there is a two component jet structure consisting of a conical mass-dominated outflow we designated the "funnel wall jet" and a low density axial jet dominated by Poynting flux. In Ref. 41 we followed up on these first results by computing a detailed series of simulations using different black hole spins. The Poynting flux jet is produced by electromagnetic fields that rotate at a rate tied closely to that of the black hole. The energy source for this jet is therefore the rotating space time of the Kerr black hole, a form of the so-called Blandford–Znajek process.[42] When the spin parameter a/M of the black hole exceeds ≈ 0.9, the energy carried to infinity by these outflows can be comparable to the nominal radiative efficiency predicted in standard disk models. Jet formation depends on the ability of the disk to eject a magnetic field into the empty funnel region along the black hole's axis. Because the magnetorotational instability is capable of exponentially amplifying weak pre-existing magnetic fields, it might be hoped that this would be a generic process. We have explored the degree to which the character of the flows

around black holes depends on the topology of the field imposed in the initial conditions. Although we find that the qualitative properties of the accretion disk are nearly independent of field topology, jet launching is very sensitive to it; a sense of vertical field consistent for at least an inner disk inflow time is essential to the support of strong jets.[43]

Ultimately we wish to connect these simulations to observations. Although it is not yet possible to do fully global time-dependent radiation transport in disk models, some observational implications can be investigated using simple emission and absorption models coupled with relativistic ray tracing.[44] Improved understanding of the physics of hot magnetized plasmas will aid greatly in connecting dynamics to diagnostics.

VI. NEW EXPERIMENTAL POSSIBILITIES FOR MEASURING PLASMA GEOMETRY THROUGH OPACITY MEASUREMENTS

The idea that line ratios could be used as a geometry diagnostic started with the work of Kerr *et al.*,[45] in which they resolved an outstanding puzzle that had arisen in previous theoretical work by Bhatia and co-workers.[46–48] Previously it had been expected that if an emission line in a plasma becomes optically thick by increasing the plasma size (for the same density) then the ratio of that line's intensity to the intensity of another line that remains optically thin would decrease. Bhatia and co-workers showed, using an escape factor method of accounting for optical depth, that in certain cases the ratio would *increase*. They did not, however, explain how this apparently counterintuitive result came about. In the paper of Kerr *et al.*[45] Bhatia's calculations were repeated, this time using a more sophisticated model of the radiation transport [a model called CRETIN (Refs. 49 and 50)] that calculated the radiation transport in the plasma in a manner that was fully self-consistent with the calculation of the population kinetics. Kerr *et al.*[45] reproduced Bhatia's results almost exactly and showed that the puzzle did not arise from the use of the escape factor method to calculate radiation transfer (in fact the CRETIN calculations confirmed the accuracy of the escape factor technique). The CRETIN calculations did, however, expose the fundamental physics behind why the line ratio can rise with increasing optical depth, or what is equivalent, why the intensity ratio between an optically thick line and the same line calculated ignoring optical depth effects can rise above 1. This can occur because Bhatia and co-workers had chosen a particular angle of observation of the plasma (which they took to be a slab extending to all distances in the (x,y) plane but with finite depth in the z-axis-z_0). Bhatia and co-workers took the angle to be perpendicular to the face of the plasma (which here we shall subsequently call 0°). Kerr *et al.*[45] noted, through CRETIN calculations, that the line intensity ratio (thick/thin) falls away from a value greater than 1 as the angle moves away from the perpendicular (increases from 0°). The origin of the effect can now be seen to be due to the fact that an ion in the upper state of the transition is pumped in the optically thick case by photons traversing the plasma at many different angles. A beautiful, but little known theorem of geometry due to Dirac and co-workers[51,52] states that the mean chord through any convex body is given by $4V/A$ (where V is the volume and A is the area of the body). For the planar plasma we are considering, that results in a mean chord length of $2z_0$ (twice the perpendicular distance from one side to the other). Such a mean chord would be at an angle of 60° to the normal. So, for an observation angle of 0°, the upper state is pumped by plasma which is longer than that through which it is interrogated. The effect is that the line intensity is greater than the optically thin value, but that it drops to the thin value as the observation angle increases to 60°, almost exactly as is calculated by CRETIN.

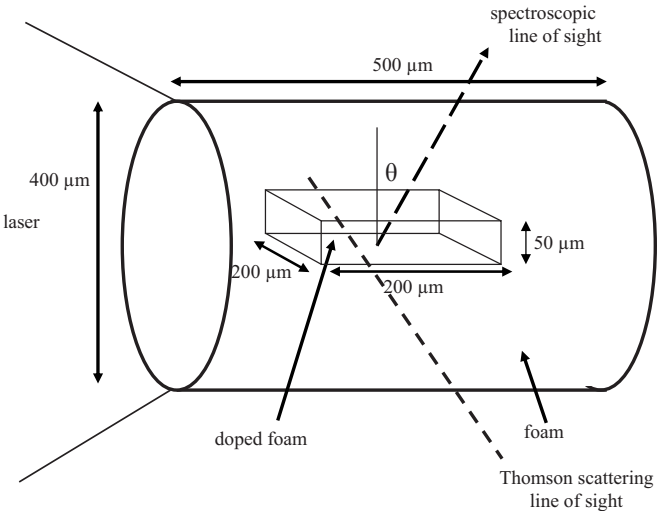

FIG. 11. Schematic of a possible experiment in which a laser heats a block of aerogel foam at subcritical density into which is doped the emitting material (for this experiment we choose the doped material to be sodium) in a region of a chosen (in this case planar) geometry. Thomson scattering determines the electron and ion temperature (both are needed: the first determines the kinetics and the second determines the line width and thereby the optical depth). The doped region remains unaffected until it is disrupted by the rarefaction wave that moves inwards from the outside of the foam. Calculations show that for sodium doped into the central region, the kinetics reach a steady state in a few hundreds of picoseconds which shows that the doped plasma has long enough to reach a steady state before it is disrupted. The spectroscopic observation of the line intensity ratio is conducted at a variety of angles θ and for a number of different dopant concentrations.

This insight has been extended in a further paper[53] using an analytic approach to consider several geometries (plane, cylinder and sphere) where the observer is far away from the plasma and cannot discriminate spatially. This paper suggests that an enhancement of optically thick to optically thin emission can be used to discriminate between different possible geometries of plasma and between different orientations of the plasma to the observer. This might be particularly valuable in observations of distant astrophysical plasma sources where it is not possible to spatially resolve the plasma but it is possible to spectrally resolve the spatially-integrated emission. Indeed recently Rose *et al.*[54] reported the first evidence for an enhancement of optically thick to thin emission from measurements of Fe XVII lines during a period of observation of the star EV Lac using the XMM-Newton satellite and more observations are planned.

Rose *et al.*[55] describes an outline design of an experiment using a high-power laser to check our theoretical mod-

eling. The experiment that is proposed builds on recent work conducted using the NIKE laser. In these studies Back *et al.*[56] demonstrated that it was possible to heat a low density (few mg/cm^3) aerogel foam target to electron temperatures of over 500 eV with good uniformity. This was accomplished by driving a supersonic heating wave through the foam producing a plasma of known density that disassembles through the progress of a rarefaction wave starting at the outside of the plasma. By doping the foam with an element in a central region, a plasma of known uniform temperature (diagnosed using Thomson scattering) and initial density, known composition and selected geometry can be produced in the laboratory. A schematic of the experiment is shown in Fig. 11. Observation of a line intensity ratio (thick/thin) as a function of increasing dopant concentration and angle will allow us to produce the analog of the astrophysical situation described by Kerr *et al.*[45] and will thereby allow us to check our modeling.

VII. CONCLUSIONS

We have presented a brief review on the astrophysics and laboratory experiments relevant for the dynamics of accreting compact objects, the atomic kinetics of photoionized plasmas, and radiation transport and opacity effects. On the one hand, new numerical simulation techniques permit the modeling of accreting disk dynamics with a level of unprecedented detail. On the other hand, current atomic and radiation physics modeling codes permit critical analysis and interpretation of spectral measurements from both astrophysical and laboratory plasmas that suggest new insights into photoionized plasma atomic kinetics, radiation transport, and stellar opacities.

ACKNOWLEDGMENTS

We thank the Z dynamic *Hohlraum*, accelerator, diagnostics, materials processing, target fabrication, and wire array teams for invaluable and dedicated technical assistance. We are grateful to R. J. Leeper, T. A. Mehlhorn, J. L. Porter, and M. K. Matzen for support and encouragement. Sandia is a multiprogram laboratory operated by Sandia Corporation, a Lockheed Martin Company, for the U.S. Department of Energy under Contract No. DE-AC04-94AL85000. The work of R.C.M. was supported by the DOE/SSAA under Grant No. DE-FG52-06NA27587. The work of J.F.H. was supported by the NSF under Grant No. PHY-0205155 and the NASA under Grant No. NNG04GK77G.

[1] M. K. Matzen, Phys. Plasmas **4**, 1519 (1997).
[2] J. E. Bailey, G. Chandler, D. Cohen, M. Cuneo, M. Foord, R. Heeter, D. Jobe, P. Lake, J. MacFarlane, T. Nash, D. Nielson, R. Smelser, and J. Torres, Phys. Plasmas **9**, 2186 (2002).
[3] M. E. Cuneo, D. Sinars, E. Waisman, D. Bliss, W. Stygar, R. Vesey, R. Lemke, I. Smith, P. Rambo, J. Porter, G. Chandler, T. Nash, M. Mazarakis, R. Adams, E. Yu, K. Struve, and T. Mehlhorn, Phys. Plasmas **13**, 056318 (2006).
[4] J. E. Bailey, G. Chandler, R. Mancini, S. Slutz, G. Rochau, M. Bump, T. Burris-Mog, G. Cooper, G. Dunham, I. Golovkin, J. Kilenny, P. Lake, R. Leeper, R. Lemke, J. MacFarlane, T. Mehlhorn, T. More, T. Nash, A. Nikroo, D. Nielsen, K. Peterson, C. Ruiz, D. Schroen, D. Steinman, and W. Varnum, Phys. Plasmas **13**, 056301 (2006).
[5] S. Basu and H. M. Antia, Phys. Rep. **457**, 217 (2008).
[6] J. N. Bahcall, A. M. Serenelli, and M. Pinsonneault, Astrophys. J. **614**, 464 (2004); S. Basu and H. M. Antia, Astrophys. J. Lett. **606**, L85 (2004); H. M. Antia and S. Basu, *ibid.* **620**, L129 (2005); J. N. Bahcall, A. M. Serenelli, and S. Basu, *ibid.* **621**, L85 (2005).
[7] J. J. MacFarlane, I. E. Golovkin, P. R. Woodruff, D. R. Welch, B. V. Oliver, T. A. Mehlhorn, and R. B. Campbell, *Proceedings of the 2003 Inertial Fusion Science and Applications Conference*, edited by B. A. Hammel, D. D. Meyerhofer, J. Meyer-ter-Vehn, and H. Azechi (American Nuclear Society, LaGrange Park, IL, 2004), p. 457.
[8] T. S. Perry, S. Davidson, F. Serduke, D. Bach, C. Smith, J. Foster, R. Doyas, C. Iglesias, F. Rogers, J. Abdallah, Jr., R. Stewart, J. Kilkenny, and R. W. Lee, Phys. Rev. Lett. **67**, 3784 (1991); P. T. Springer, K. Wong, C. Iglesias, J. Hammer, J. Porter, A. Toor, W. Goldstein, B. Wilson, F. Rogers, C. Deeney, D. Dearborn, C. Bruns, J. Emig, and R. Stewart, J. Quant. Spectrosc. Radiat. Transf. **58**, 927 (1997).
[9] T. S. Perry, P. Springer, D. Fields, D. Bach, F. Serduke, C. Iglesias, F. Rogers, J. Nash, M. Chen, B. Wilson, W. Goldstein, B. Rosznai, R. Ward, J. Kilkenny, R. Doyas, L. Da Silva, C. Back, and R. Cauble, Phys. Rev. E **54**, 5617 (1996).
[10] J. E. Bailey, G. Rochau, C. Iglesias, J. Abdallah, Jr., J. J. MacFarlane, I. Golovkin, P. Wang, R. C. Mancini, P. W. Lake, T. C. Moore, M. Bump, O. Garcia, and S. Mazevet, Phys. Rev. Lett. **99**, 265002 (2007).
[11] J. E. Bailey, G. A. Rochau, R. C. Mancini, C. A. Iglesias, J. J. MacFarlane, I. E. Golovkin, J. C. Pain, F. Gilleron, C. Blancard, Ph. Cosse, G. Faussurier, G. A. Chandler, T. J. Nash, D. S. Nielsen, and P. W. Lake, Rev. Sci. Instrum. **79**, 113104 (2008).
[12] C. A. Iglesias and F. J. Rogers, Astrophys. J. **464**, 943 (1996).
[13] S. Mazevet and J. Abdallah, Jr., J. Phys. B **39**, 3419 (2006).
[14] P. Renaudin, L. Lecherbourg, C. Blancard, P. Cosse, G. Faussurier, P. Audebert, S. Bastiani-Ceccoti, J. P. Geindre, and R. Shepherd, AIP Conf. Proc. **926**, 24 (2007).
[15] T. R. Kallman and R. McCray, Astrophys. J., Suppl. Ser. **50**, 263 (1982); D. A. Liedahl, *X-Ray Spectroscopy in Astrophysics: Lectures Held at the Astrophysics School X* (Springer, Amsterdam, 1999), Vol. 520, p. 189; *Spectroscopic Challenges of Photoionized Plasmas*, Astronomical Society of the Pacific Conference Series Vol. 247, edited by G. Ferland and D. W. Savin (Sheridan, Chelsea, MI, 2001).
[16] C. B. Tarter, W. Tucker, and E. E. Salpeter, Astrophys. J. **156**, 943 (1969).
[17] R. F. Heeter, J. Bailey, M. Cuneo, J. Emig, M. Foord, P. Springer, and R. Thoe, Rev. Sci. Instrum. **72**, 1224 (2001); M. E. Foord, R. Heeter, P. van Hoof, R. Thoe, J. Bailey, H. Chung, D. Liedahl, K. Fournier, G. Chandler, V. Jonauskas, R. Kisielius, L. Mix, C. Ramsbottom, P. Springer, F. Keenan, S. Rose, and W. Goldstein, Phys. Rev. Lett. **93**, 055002 (2004).
[18] P. A. M. Van Hoof, M. E. Foord, R. F. Heeter, J. E. Bailey, H.-K. Chung, M. E. Cuneo, W. H. Goldstein, V. Jonauskas, F. P. Keenan, R. Kisielius, D. A. Liedahl, C. Ramsbottom, S. J. Rose, P. T. Springer, and R. S. Thoe, Astrophys. Space Sci. **298**, 147 (2005).
[19] S. Rose, P. van Hoof, V. Joansukas, F. Keenan, R. Kisielius, C. Ramsbottom, M. Foord, R. Heeter, and P. Springer, J. Phys. B **37**, L337 (2004).
[20] J. E. Bailey, D. Cohen, G. Chandler, M. Cuneo, M. Foord, R. Heeter, D. Jobe, P. Lake, D. Liedahl, J. MacFarlane, T. Nash, D. Nielson, R. Smelser, and W. Stygar, J. Quant. Spectrosc. Radiat. Transf. **71**, 157 (2001).
[21] D. H. Cohen, J. J. MacFarlane, and J. E. Bailey, Rev. Sci. Instrum. **74**, 1962 (2003).
[22] H. G. Wei, J. R. Shi, G. Zhao, Y. Zhang, Q. L. Dong, Y. T. Li, S. J. Wang, J. Zhang, Z. T. Liang, J. Y. Zhang, T. S. Wen, W. H. Zhang, X. Hu, S. Y. Liu, Y. K. Ding, L. Zhang, Y. J. Tang, B. H. Zhang, Z. J. Zheng, H. Nishimura, S. Fujioka, F. L. Wang, and H. Takabe, "Opacity studies of silicon in radiatively heated plasmas," Astrophys. J. (in press).
[23] J. Zeng, G. Zhao, and J. Yuan, Phys. Rev. E **70**, 027401 (2004).
[24] M. F. Gu, Astrophys. J. **597**, 1241 (2003).
[25] K. Kawashima and S. Kitamoto, Publ. Astron. Soc. Jpn. **48**, L113 (1996).
[26] F. Paerels, J. Cottam, M. Sako, D. A. Liedahl, A. C. Brinkman, R. L. J. van der Meer, J. S. Kaastra, and P. Predehl, Astrophys. J. Lett. **533**, L135 (2000).
[27] N. Miyanaga, Proc. SPIE **2633**, 183 (1995).
[28] A. Bar-Shalom, M. Klapisch, and J. Oreg, J. Quant. Spectrosc. Radiat. Transf. **71**, 169 (2001).

[29]F. L. Wang, S. Fujioka, H. Nishimura, D. Kato, Y. Li, G. Zhao, J. Zhang, and H. Takabe, Phys. Plasmas **15**, 073108 (2008).
[30]S. Kaspi, W. Brandt, I. George, H. Netzer, D. Crenshaw, J. Gabel, F. Harmann, M. Kraiser, A. Koratkar, S. Kraemer, G. Kriss, S. Mathur, R. Mutchosky, K. Nandra, B. Peterson, J. Shields, T. Turner, and W. Zheng, Astrophys. J. **574**, 643 (2002).
[31]R. A. Remillard and J. E. McClintock, Annu. Rev. Astron. Astrophys. **44**, 49 (2006).
[32]N. I. Shakura and R. A. Sunyaev, Astron. Astrophys. **24**, 337 (1973).
[33]I. D. Novikov and K. S. Thorne, in *Black Holes: Les Astres Occlus*, edited by C. DeWitt and B. DeWitt (Gordon and Breach, New York, 1973), p. 343.
[34]S. A. Balbus and J. F. Hawley, Rev. Mod. Phys. **70**, 1 (1998).
[35]J.-P. De Villiers and J. F. Hawley, Astrophys. J. **589**, 458 (2003).
[36]J.-P. De Villiers, J. F. Hawley, and J. H. Krolik, Astrophys. J. **599**, 1238 (2003).
[37]J. H. Krolik, J. F. Hawley, and S. Hirose, Astrophys. J. **622**, 1008 (2005).
[38]J. C. McKinney and C. F. Gammie, Astrophys. J. **611**, 977 (2004).
[39]J. F. Hawley, K. Beckwith, and J. H. Krolik, Astrophys. Space Sci. **311**, 117 (2007).
[40]S. Hirose, J. H. Krolik, J. P. De Villiers, and J. F. Hawley, Astrophys. J. **606**, 1083 (2004).
[41]J. F. Hawley and J. H. Krolik, Astrophys. J. **641**, 103 (2006).
[42]R. D. Blandford and R. L. Znajek, Mon. Not. R. Astron. Soc. **179**, 433 (1977).
[43]K. Beckwith, J. F. Hawley, and J. H. Krolik, Astrophys. J. **678**, 1180 (2008).
[44]J. D. Schnittman, J. H. Krolik, and J. F. Hawley, Astrophys. J. **651**, 1031 (2006).
[45]F. M. Kerr, S. J. Rose, J. S. Wark, and F. P. Keenan, Astrophys. J. Lett. **613**, L181 (2004).
[46]A. K. Bhatia and J. L. R. Saba, Astrophys. J. **563**, 434 (2001).
[47]S. O. Kastner and A. K. Bhatia, Astrophys. J. **553**, 421 (2001).
[48]A. K. Bhatia and S. O. Kastner, Astrophys. J. **516**, 482 (1999).
[49]H. Scott and R. W. Mayle, Appl. Phys. B: Lasers Opt. **58**, 35 (1994).
[50]H. Scott, J. Quant. Spectrosc. Radiat. Transf. **71**, 689 (2001).
[51]P. A. M. Dirac, Technical Report No. MS-D-5, 1943.
[52]P. A. M. Dirac, K. Fuchs, R. Peierls, and P. Preston, Technical Report No. MS-D-5, 1943.
[53]F. M. Kerr, S. J. Rose, J. S. Wark, and F. P. Keenan, Astrophys. J. **629**, 1091 (2005).
[54]S. J. Rose, M. Matranga, M. Mathioudakis, F. P. Keenan, and J. S. Wark, Astron. Astrophys. **483**, 887 (2008).
[55]S. J. Rose, J. S. Wark, and F. P. Keenan, "New experimental possibilities for measuring plasma geometry through opacity measurements," Astrophys. Space Sci. (in press)
[56]C. A. Back, U. Feldman, J. L. Weaver, J. F. Seely, C. Constantin, G. Holland, R. W. Lee, H.-K. Chung, and H. A. Scott, J. Quant. Spectrosc. Radiat. Transf. **99**, 21 (2006).